ACS APPLIED MATERIALS & INTERFACES

Research Article

www.acsami.org

Genetically Engineered Phage-Templated MnO_2 Nanowires: Synthesis and Their Application in Electrochemical Glucose Biosensor Operated at Neutral pH Condition

Lei Han,[†,‡] Changxu Shao,[†,‡] Bo Liang,[‡] and Aihua Liu*[,†]

[†]Institute for Biosensing, and College of Chemistry and Chemical Engineering, Qingdao University, Qingdao 266071, China

[‡]Laboratory for Biosensing, Qingdao Institute of Bioenergy & Bioprocess Technology, Chinese Academy of Sciences, 189 Songling Road, Qingdao 266101, China, and

University of Chinese Academy of Sciences, 19A Yuquan Road, Beijing 100049, China

ABSTRACT: To conveniently obtain one-dimensional MnO_2 nanowires (NWs) with controlled structure and unique properties for electron transfer, the genetically engineered M13 phages were used as templates for precise nucleation and growth of MnO_2 crystals in filamentous phage scaffolds, via the spontaneous oxidation of Mn^{2+} in alkaline solution. It was found that the morphology of NWs could be tailored by the surface charge of M13 mutants. MnO_2 crystals were uniformly distributed on the surface of negatively charged tetraglutamate-fused phage (M13-E4), significantly different from irregular MnO_2 agglomeration on the weakly negatively charged wild-type phage and positively charged tetraarginine-fused phage. The as-synthesized M13-E4@MnO_2 NWs could catalyze the electro-oxidation of H_2O_2 at neutral pH. To demonstrate the superiority of the electrocatalytic activity in the solution containing plenty of chloride ions at neutral pH, both glucose oxidase and as-prepared MnO_2 NWs were used for fabricating the glucose biosensor. The proposed biosensor showed a wide linear range (5 μM to 2 mM glucose), a low limit of detection of 1.8 μM glucose (S/N = 3), good interassay and intra-assay reproducibility and satisfactory storage stability. Due to the superiorities of synthesis and electrochemical performance, the as-prepared MnO_2 NWs are promising for applications in electrocatalysis, electrochemical sensor, and supercapacitor.

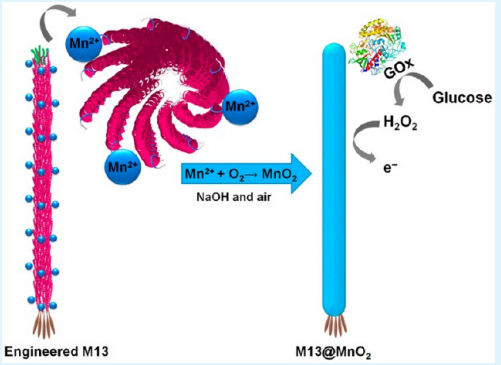

KEYWORDS: *MnO_2 nanowires, biotemplate synthesis, phage display, electrochemical glucose biosensor, neutral pH*

1. INTRODUCTION

As a kind of attractive transition metal oxide, manganese dioxide (MnO_2) with different morphologies has been widely studied on the field of chemical catalysis,[1] electrocatalysis,[2] photocatalysis,[3] and supercapacitor,[4] due to its high catalytic activity, environmental friendliness, and nontoxicity.[2,5] Among the different morphologies of MnO_2, one-dimensional (1D) nanostructured morphologies have attracted more and more interests for electrochemical application (such as supercapacitor, ion battery, and electrochemical sensor), due to the controlled structure for electron transfer, quantum size effect, and surface effect.[6−10] So far, various MnO_2 nanomaterials with 1D morphology such as nanowires (NWs),[9,11,12] nanorods,[13,14] nanoneedles,[9] nanotubes,[7,15,16] and nanofibers[17] have been prepared by conventional methods. For example, Cheng et al. synthesized MnO_2 nanowires, nanorods, and nanoneedles by hydrothermal routes.[9] Li et al. reported that MnO_2 nanotubes with large surface area were synthesized under hydrothermal conditions by an interesting exfoliation and scrolling process.[7] Xie et al. prepared MnO_2 nanorods via heterogeneous catalytic reactions at high temperature.[18] Dongale et al. prepared the MnO_2 nanofiber films by electrodeposition method.[17] However, these synthesis methods generally require complex instrumentation, heating processes, harmful organic reagents, and strong oxidants such as $KMnO_4$ and $(NH_4)_2S_2O_8$, which might further restrict their application. In addition, it is still difficult to precisely design and control the morphology. Furthermore, there are some disadvantages on MnO_2-based electrochemical sensor. On one hand, like most metal[19] and metal oxides,[20−22] many MnO_2 nanomaterials also exhibit the electrocatalytic activity at the alkaline pH, such as MnO_2 nanoparticles (NPs)[23,24] and MnO_2 NWs.[11,25] On the other hand, the response time and limit of detection still need to be improved on many MnO_2-based enzymatic biosensors.[26] To overcome these challenges, we intended to improve the 1D MnO_2 nanomaterials with controllable morphology and electrocatalytic activity at the neutral pH by a facile and green synthetic method.

Nature provides us an enormous library of natural biomaterials with an astonishing variety of sophisticated

Received: March 17, 2016
Accepted: May 12, 2016

ACS Publications © XXXX American Chemical Society

DOI: 10.1021/acsami.6b03266
ACS Appl. Mater. Interfaces XXXX, XXX, XXX−XXX

nanostructures, which are hard to be obtained even by the advanced synthesis technologies.[27] As the requirements for nanomaterials with controllable morphologies and improved performances are becoming increasingly significant, researchers have been exploring the potential of different biomaterials for scaffolds to fabricate novel types of nanostructures.[28] Also, then, the biotemplate synthesis method emerged, where the natural biomaterials such as DNA,[29] protein,[30] virus,[31] bacteria,[32] diatom,[33] and leaf[20] were used as templates of biomineralization to nucleate and grow inorganic crystals in limited space under mild conditions.[27,34] The wild-type M13 phage is a kind of filamentous virus (about 6.5 nm in diameter and about 880 nm in length),[35] composed of about 2700 copies of major coat proteins (pVIII) helically and closely wrapped around a circular single-stranded DNA and 5 copies each of minor coat proteins (pIII, pVI, pVII, and pIX) at both ends of the phage.[36,37] The functionality of coat proteins can be realized by genetic engineering and has been used successfully as templates for precisely positioned nucleation and growth of nanocrystals.[38] Mao et al. reported the engineered M13-based scaffolds for the synthesis of CoPt and FePt nanowires (NWs).[39] Nam et al. used the engineered M13 templates to synthesize and assemble Co_3O_4 NWs for lithium-ion battery electrodes.[36] Lee et al. equipped the viral major coat proteins with peptides capable of nucleating amorphous iron phosphate ($FePO_4$) for fabricating lithium-ion battery cathodes.[40] Nam et al. reported the spontaneous reduction of silver ions into nanostructures by M13 surface-displayed peptides.[41] Lee et al. developed a simple synthetic route of Au NWs by surfactant-mediated biomineralization of a genetically engineered M13 phages with specific Au binding peptides, and found that Au NWs were active for electrocatalytic oxidation of carbon monoxide.[42] In our previous work, virus-based nanocomposite films were prepared by layer-by-layer assembly of cationic genetically engineered M13 and anionic Au nanoparticles (NPs) through the electrostatic interaction.[43] However, noble metals and transition metal oxides are not confined to the above cases and new kinds of inorganic NWs based on the M13 templates still need to be developed for a variety of applications.

Here, we report the genetically engineered M13 phages acting as biotemplates for nucleation and growth of MnO_2 crystals in filamentous phage scaffolds. The morphology of NWs could be tailored by the surface charge of M13 mutants. The MnO_2 NWs were formed onto negatively charged tetraglutamate-fused phage. The fabricated MnO_2 NWs exhibited the amperometric response for H_2O_2 at neutral pH. To demonstrate the superiority of the electrocatalytic activity at neutral pH, both glucose oxidase (GOx, EC No. 1.1.3.4) and as-prepared MnO_2 NWs were used for fabricating the glucose biosensor.

2. MATERIALS AND METHODS

2.1. Chemicals and Materials. The oligonucleotides were synthesized by BGI Tech (Shenzhen, China). FastDigest enzymes (*Eco*RI and *Bam*HI) were purchased from Thermo Scientific. M13KO7 helper was purchased from New England BioLabs (Beijing, China). Isopropyl β-D-thiogalactoside (IPTG), ampicilin, and kanamycin were purchased from Takara Biotechnology Co., Ltd. (Dalian, China). Polyethylene glycol (PEG) was purchased from Solarbio (Beijing, China). Manganese acetate ($MnAc_2$), hydrogen peroxide (H_2O_2, 30%), and glucose were purchased from Sinopharm Chemical Reagent Co., Ltd. (Shanghai, China). GOx was purchased from Toyobo Co., Ltd. (Osaka, Japan). Nafion (perfluorinated ion-exchange resin, 5 wt % solution in a mixture of lower aliphatic alcohols and water) were purchased from Sigma-Aldrich (St. Louis, MO). Tryptone and yeast extract were purchased from Oxoid (Basingtstoke, U.K.). All other reagents were of analytical grade, and all aqueous solutions were prepared with Milli-Q water (18.2 MΩ cm).

2.2. M13 Phage Engineering and Purification. To display tetraglutamic acid (−EEEE) on the N-terminus of the pVIII protein on M13 phage (producing so-called M13-E4), a small DNA duplex encoding the amino acids was made using an oligonucleotide 5′-CGCG*GGATCC*TCTCCTCCTCCTCC*GAATTC*CCGG-3′ (the italic type represents the restriction sites) and the extension primer, 5′-CCGGGAATTCGGAGGAGGA-3′. The duplex was digested with *Eco*RI and *Bam*HI and ligated into PC89 phasmid, and confirmed by DNA sequencing.[41] For the tetraarginine-fused phage (M13-R4), the above-mentioned experimental process was conducted except for using an oligonucleotide 5′-CGCG*GGATCC*TCCCTCCTCCTCCT-*GAATTC*CCGG-3′ and the extension primer CCGGGAATTCAG-GAGGAGG.

After the transformation of competent cells, *E. coli* TG1 containing the engineered PC89 phagemids were inoculating into 2 × YT broth (16 g/L tryptone, 10 g/L yeast extract, 5 g/L NaCl) with ampicilin (50 μg/mL). After the shaking culture (200 rpm) at 37 °C overnight, 400 μL of culture was added into 40 mL of fresh 2 × YT broth. The phagemids were rescued by superinfection of *E. coli* TG-1 with M13KO7 helper phage (10^8 virions/mL), and peptide display was induced by 1 mM IPTG with vigorous shaking (300 rpm) at 37 °C overnight with kanamycin (25 μg/mL) selection.[36]

After the incubation for 20 min at 70 °C, the culture was centrifuged for 15 min at 5000 rpm to remove the cell precipitates. A 0.15 volume of PEG/NaCl was added into the supernatants. After the incubation for 1 h in an ice bath, the mixture was centrifuged for 5 min at 12 000 rpm to remove the supernatants. After the resuspension by phosphate buffered saline (PBS), the solution was centrifuged for 5 min at 12 000 rpm to remove the insoluble substances. The concentration of phage was calculated using the following formula: virions/mL = $(A_{269} - A_{320}) \times 6 \times 10^{16}$/number of bases per virion, where A_{269} and A_{320} are denoted as the absorbance at 269 and 320 nm, respectively.[44]

2.3. Synthesis of M13-E4@MnO_2 NWs. Typically, 1 μL of M13-E4 (10^{14} virions/mL) was added into 1 mL $MnAc_2$ aqueous solution (1 mM). After stirring for 1 h at room temperature, diluted NaOH solution was added into the mixture solution to adjust the pH to 9−10, and the color of the solution immediately changed to brown color. After stirring for 6−8 h, the M13-E4@MnO_2 NWs were filtered by 0.02 μm membrane to remove unreacted $MnAc_2$ and NaOH. After washing with water, the prepared NWs were dried and stored at 4 °C.[45]

2.4. Preparation of the Electrochemical Sensor. Before surface modification, the glassy carbon electrode (GCE, 3 mm in diameter) was polished with 0.05 μm alumina slurry, rinsed with water, and dried in air. To prepare Nafion/MnO_2 NWs/GCE sensor, 5 μL of 2 mg/mLM13-E4@MnO_2 NW (MnO_2 NWs for short) aqueous suspension was dropped onto the surface of the inverted electrode and dried in air. Finally, 5 μL of Nafion solution (0.1 wt % in ethanol) was dropped onto the electrode in order to entrap NWs. To fabricate Nafion/GOx/MnO_2 NWs/GCE sensor, 5 μL of 2 mg/mLMnO_2 NWs aqueous suspension, 5 μL of GOx solution (10 mg/mL), and 5 μL of Nafion solution (0.1 wt % in ethanol) were dropped onto the surface of the inverted electrode in sequence and dried in air. Before use, the modified electrodes were washed with water to remove any loosely combined modifiers.

2.5. Apparatus and Electrochemical Measurements. The morphology of the as-prepared NWs was observed by the transmission electron microscopy (TEM, HITACHI H-7650). The elementary composition and valence state were analyzed by X-ray photoelectron spectroscopy (XPS, Thermo Fisher ESCALAB 250Xi). The zeta potential was measured by Zetasizer Nano ZSP (Malvern Instruments Ltd., Worcestershire, U.K.). Electrochemical measurements were performed on a CHI 660E electrochemical workstation (CH Instruments, Chenhua, Shanghai, China). All electrochemical measure-

DOI: 10.1021/acsami.6b03266
ACS Appl. Mater. Interfaces XXXX, XXX, XXX−XXX

ments were carried out at room temperature in a conventional three-electrode system with a modified GCE as the working electrode, a platinum wire as the counter electrode, and a saturated calomel electrode (SCE) as the reference electrode. For chronoamperometry, all measurements were performed at appropriate potential on successive injection of analytes in stirring PBS solution, and the effect of dilution on the final concentration had been taken into consideration.

3. RESULTS AND DISCUSSION

3.1. Synthesis and Characterizationof MnO_2 NWs.

M13-E4@MnO_2 NWs were obtained by adding NaOH into the mixture solution containing M13-E4 and $MnAc_2$ in air at room temperature (Scheme 1). First, E4-tagged pVIII proteins of

Scheme 1. Schematic Diagram of Engineered M13-Mediated Synthesis of MnO_2 NWs (Not to Scale)

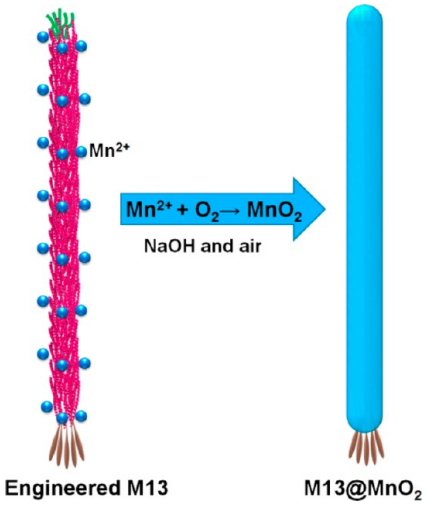

M13-E4 provided carboxyl groups for specific affinity with Mn^{2+}. Second, after adding NaOH in transparent solution containing M13 and Mn^{2+}, brown hydrated manganese dioxide $MnO(OH)_2$ was formed on the surface of M13-E4 by oxidation of Mn^{2+} in air ($2Mn^{2+}(aq) + 4OH^-(aq) + O_2(g) \rightarrow 2MnO(OH)_2(s)$),[46] and then unstable $MnO(OH)_2$ decayed into stable black MnO_2 ($MnO(OH)_2(s) \rightarrow MnO_2(s) + H_2O(l)$).[45] During the process, oxygen molecules were necessary for oxidation of Mn^{2+} ion, because no MnO_2 was formed when the reaction solution was deoxidized by bubbling nitrogen (data not shown). Hence, the reaction was conducted under vigorous stirring for enough concentration of dissolved O_2. Moreover, the solution still stayed transparent without NaOH (data not shown), indicating the importance of weak alkaline pH. Third, MnO_2 crystal increasingly deposited and grew on the surface of M13-E4. Finally, the black precipitate appeared with nanowire morphology after 8 h of stirring at room temperature. The mineralized phages remained the filamentous morphology with the length of about 1 ± 0.1 μm and diameter of 20−30 nm, while the M13-E4 virion had a length of about 0.9 μm and a diameter of about 6.5 nm (Figure 1). MnO_2 crystals uniformly distributed at the phage scaffolds to form nanosized walls (about 9 nm of thickness), leading to the large specific surface area of MnO_2 NWs. To confirm the existence of MnO_2, the XPS analysis of NWs was performed (Figure 2). The Mn 2p spectrum (Figure 2B) showed that the binding energy peaks of Mn $2p_{3/2}$ and Mn $2p_{1/2}$ are located at 642.2 and 653.9 eV, respectively, and the energy separation

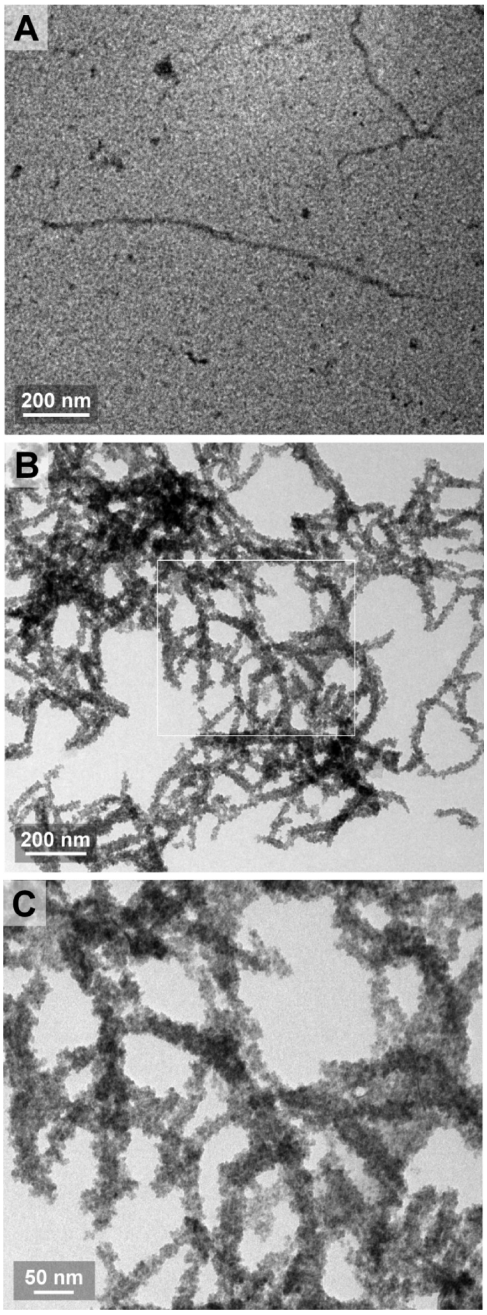

Figure 1. TEM images of negatively stained M13-E4 (A) and M13-E4@MnO_2 NWs (B and C). Part C shows the magnification of the square-marked area of part B.

(11.7 eV) between $2p_{3/2}$ and $2p_{1/2}$ was in agreement with previous reports,[47,48] implying the oxidation state of the Mn^{4+} and the formation of MnO_2 on the M13-E4 virion. Therefore, MnO_2 NWs could be obtained under mild conditions by the convenient template method with precise control of nanowire morphology. In addition, the M13 bacteriophage is a kind of high-production rate virus (200 mg/L culture)[39] in favor of large-scale production of MnO_2 NWs.

To research the influence of surface charge of M13 on biomineralization, we displayed different tetrapeptides on the N-terminus of pVIII proteins of M13 by gene engineering, which was used as a biotemplate to form MnO_2. As shown in Figure 3, a small amount of MnO_2 agglomerates appeared on the NWs from wild-type phage (M13-WT) and a large amount

DOI: 10.1021/acsami.6b03266
ACS Appl. Mater. Interfaces XXXX, XXX, XXX−XXX

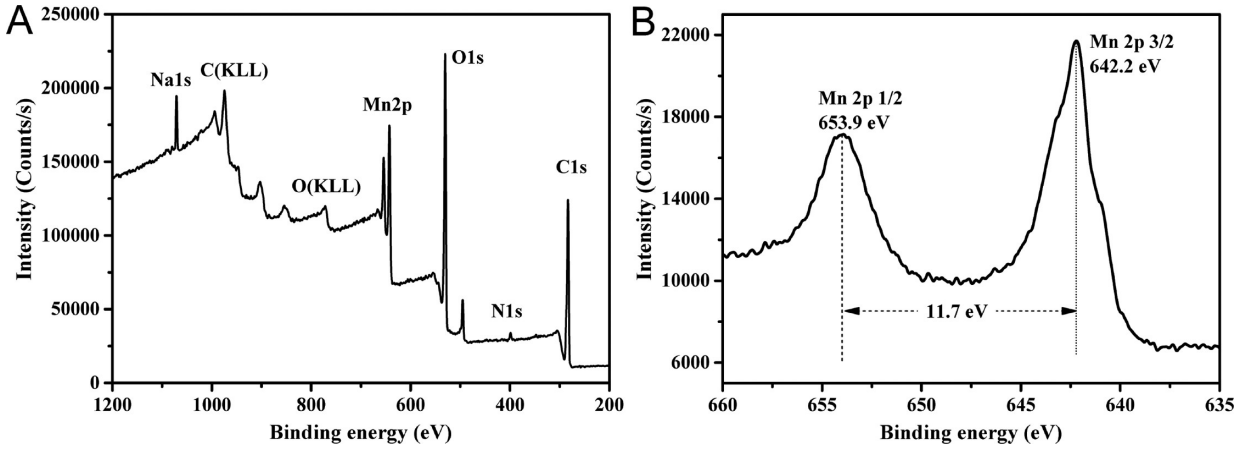

Figure 2. XPS pattern of M13-E4@MnO_2 NWs (A) and high-resolution XPS pattern of Mn 2p (B).

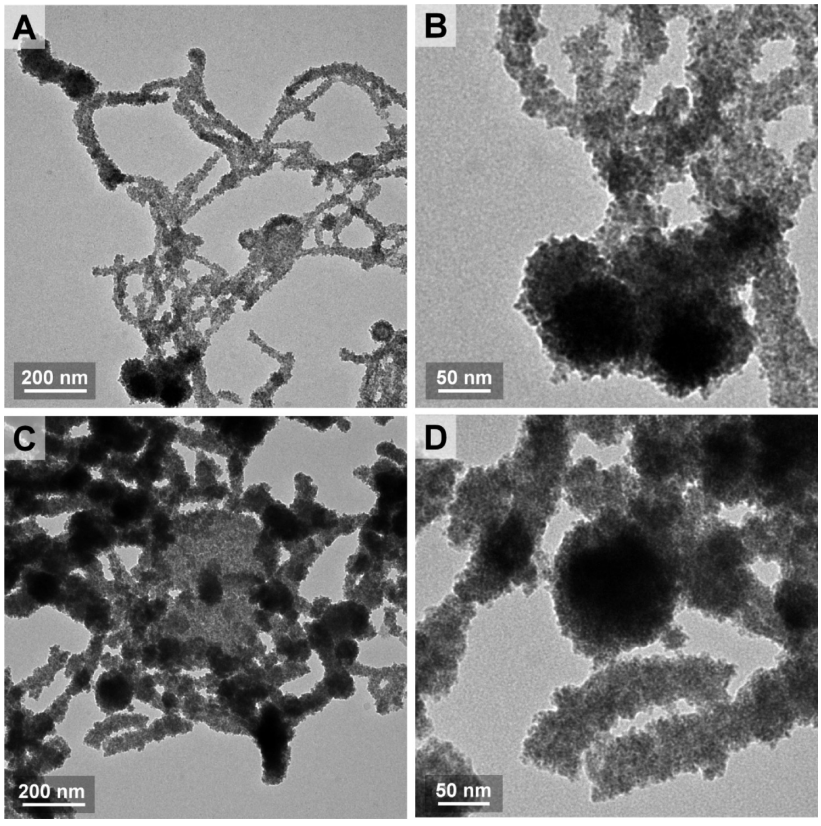

Figure 3. TEM images of phage-templated MnO_2 with WT-M13 (A, B), with M13-R4 (C, D).

of MnO_2 agglomerates appeared on the NWs from tetraarginine-fused phage (M13-R4). By contrast, MnO_2 crystals were uniformly distributed on the surface of tetraglutamate-fused phage (M13-E4) without irregular agglomeration (Figure 1), implying the easier nucleation on the M13-E4 phage surface. To explain the phenomena, the zeta potentials of M13-E4, M13-WT, and M13-R4 in the stage of incubation with Mn^{2+} for the synthesis systems of MnO_2 were detected to be −29.2, −17.9, and +1.42 mV, separately. First, the isoelectric point (pI) of glutamate is 3.22. When pH of the reaction solution was within 9−10, glutamate was negatively charged. Glutamate can bind positively charged metal ions by electrostatic interaction to facilitate the further mineralization in the laboratory,[36,40,41] and glutamate in specific proteins can regulate the nucleation of biominerals in nature.[36] So, M13-E4 was more negatively charged than M13-WT, resulting in the greater affinity of M13-E4 for Mn^{2+} than M13-WT. Second, considering that the pI of arginine is 10.76, when pH of the reaction solution was within 9−10, M13-R4 was more positively charged than M13-WT, which enabled it to repel with the positively charged Mn^{2+}. Due to the repellency for Mn^{2+} and the reduced number of nucleation sites, MnO_2 crystals were agglomerated far from the M13-R4 phage surfaces, resulting in the smaller specific surface area. Therefore, the M13-E4@MnO_2 NWs were selected for subsequent experiments.

On the other hand, the concentration of M13-E4 was critical for controlling the nanowire morphology. As the concentration

DOI: 10.1021/acsami.6b03266
ACS Appl. Mater. Interfaces XXXX, XXX, XXX−XXX

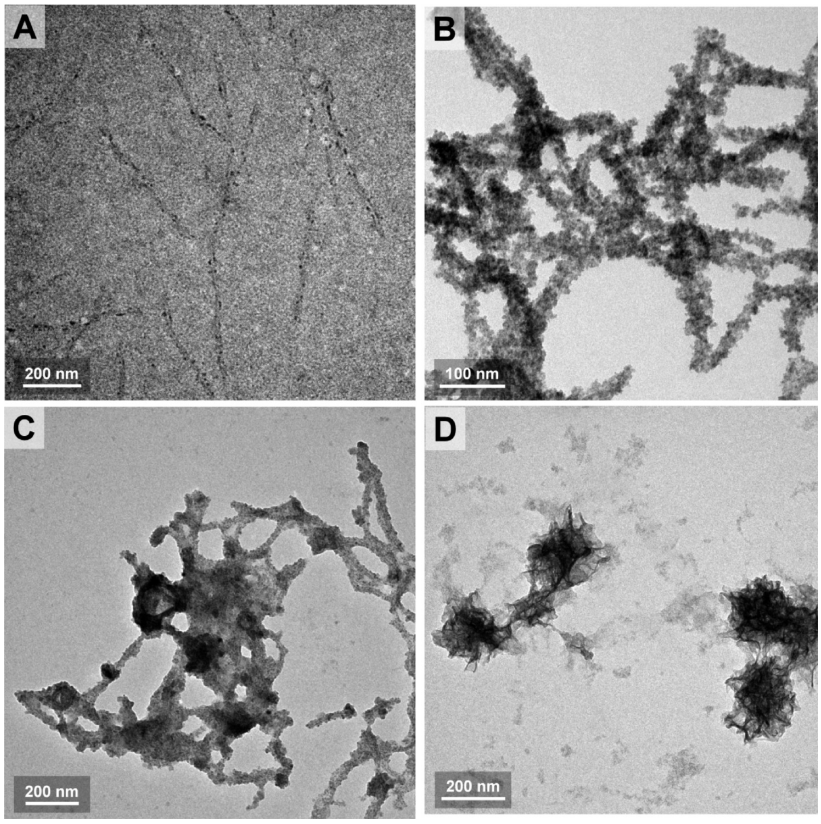

Figure 4. TEM images of MnO_2 mineralized in 1 mM $MnAc_2$ with varying M13-E4 concentrations. M13-E4 concentrations: 10^{12} (A), 10^{11} (B), 10^{10} (C), and 0 virions/mL (D).

of M13-E4 was decreased from 10^{12} to 10^{10} virions/mL in the synthesis system, the amount of MnO_2 crystals on each phage was increased (Figure 4). For the synthesis system containing 10^{12} virions/mL of M13-E4, a small amount of MnO_2 NPs were discretely deposited on M13-E4 surfaces (Figure 4A), because the M13-E4 in excessive concentration would give rise to a decrease in the number of Mn^{2+} species binding with each phage, accordingly. Thus, for the M13-E4 in moderate concentration (10^{11} virions/mL), MnO_2 crystals could uniformly distribute on the M13-E4 surface to form MnO_2 thin layers (Figure 4B). However, the M13-E4 in low concentration (10^{10} virions/mL) led to the decreased amount of nucleation sites and the cross-linking of MnO_2 NWs (Figure 4C). Compared with the M13-templated MnO_2 NWs, no nanowire structure was formed without M13-E4 templates, presumably leading to the smaller specific surface area (Figure 4D). The optimized products templated with M13-E4 (inset of Figure 4B) have greater volume than nontemplated MnO_2 (inset of Figure 4D) for the same weight, further indicating that the M13-templated MnO_2 NWs had larger specific surface area. The MnO_2 NWs formed from 10^{11} virions/mL of M13-E4 were uniform and used for the following fabrication of biosensors.

3.2. Electrochemical Oxidation of H_2O_2 at the Nafion/MnO_2 NWs/GCE. To study the electrochemical behavior of the M13-E4@MnO_2 NWs, CVs of the Nafion/MnO_2 NWs/GCE in PBS solutions (pH 7.4) containing the various concentrations of H_2O_2 were first conducted and compared with both Nafion/GCE and Nafion/template-free-MnO_2/GCE (Figure 5). At Nafion/GCE, no obvious redox peak was observed even in 0.5 mM H_2O_2, indicating electrochemical redox reaction involved with H_2O_2 could not occur at bare GCE. Fortunately, at Nafion/MnO_2 NWs/GCE, the oxidation current around +0.65 V increased significantly with the increase of H_2O_2 concentration, while the reduction current around +0.35 V did not show obvious change, indicating high electrocatalytic activity of M13-E4@MnO_2 NWs for oxidation of H_2O_2. The reactions corresponding to the oxidation current could presumably be formulated as[24] $MnO_2(s) + H_2O_2 \rightarrow Mn(OH)_2(s) + O_2(g)$; $Mn(OH)_2(s) \rightarrow MnO_2(s) + 2e^- + 2H^+(aq)$. On the contrary, only a feeble response was observed from 0 to 0.5 mM H_2O_2 at Nafion/template-free-MnO_2/GCE, indicating that the small size effect, the controlled 1D structure for electron transfer, and large surface area of NWs could remarkably improve the electrocatalytic performance of MnO_2 crystals. Interestingly, the electrocatalytic activity of the M13-E4@MnO_2 NWs was discovered at neutral pH solution (PBS buffer, pH 7.4) rather than the alkaline solution where MnO_2 and other metal oxide nanomaterials generally exhibit their electrocatalytic activity.[20,21] For the development of electroanalysis of H_2O_2, the diverse nanostructured metal oxides have been widely applied in electrochemical sensors. Pan et al. prepared a hierarchical hybrid film of MnO_2 NPs[23] and graphene-bridged MnO_2 NWs,[11] respectively, for sensitive and prompt amperometric responses to H_2O_2 in 0.1 M NaOH. Li et al. reported that a MnO_2/graphene oxide hybrid showed high electrochemical activity for the nonenzymatic detection of H_2O_2 in 0.1 M NaOH.[24] In our previous report, the leaf-templated Co_3O_4 nanostructure was synthesized for the electrochemical sensing interface for nonenzymatic detection of H_2O_2 in 0.1 M NaOH.[20] However, many reported metal-oxide-based H_2O_2 sensors need to work in an alkaline medium

DOI: 10.1021/acsami.6b03266
ACS Appl. Mater. Interfaces XXXX, XXX, XXX−XXX

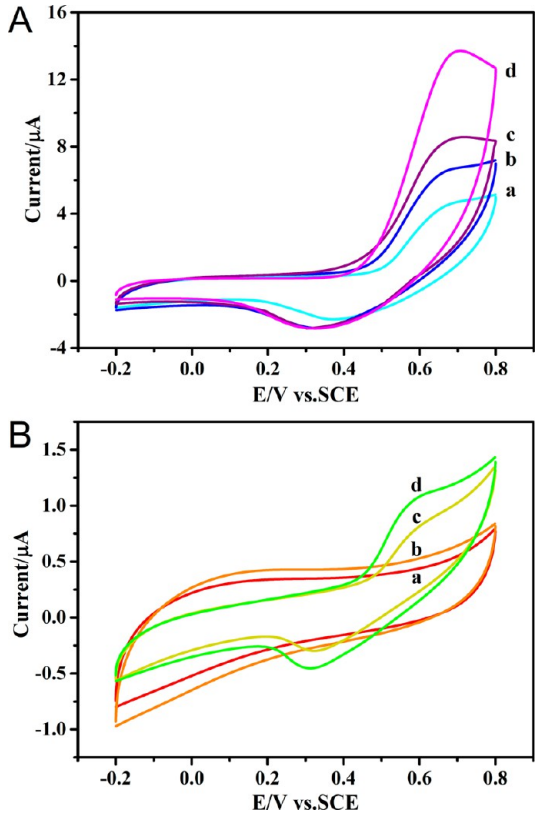

Figure 5. (A) CVs of Nafion/MnO_2 NWs/GCE in PBS (pH 7.4) containing 0 (a), 0.1 (b), 0.2 (c), 0.5 mM H_2O_2 (d). (B) CVs of Nafion/GCE in PBS (pH 7.4) containing 0 (a) and 0.5 mM H_2O_2 (b), and Nafion/template-free-MnO_2/GCE in PBS (pH 7.4) containing 0 (c) and 0.5 mM H_2O_2 (d). Scan rate, 25 mV s^{-1}.

rather than at nearly neutral conditions,[20−24] which would hinder their practical applications. The interesting electrocatalytic property of the as-prepared MnO_2 NWs at neutral pH was similar to MnO_2-modified vertically aligned multiwalled carbon nanotubes[49] and MnO_2 nanorods,[50] which would facilitate their application at neutral condition.

3.3. Electrochemical Detection of Glucose Using Nafion/GOx/MnO_2 NWs/GCE Biosensor. Considering that the M13-E4@MnO_2 NWs exhibited the electrocatalytic activity at neutral pH where GOx had optimal activity, the glucose biosensor was fabricated by dropping GOx onto the M13-E4@MnO_2-modified electrode. In the presence of oxygen molecules, GOx can catalyze the oxidation of glucose to result in the formation of gluconolactone and H_2O_2. By the detection of H_2O_2, the indirect detection of glucose could be realized. To comfirm the current response for glucose at Nafion/GOx/MnO_2 NWs/GCE biosensor, CVs were detected in PBS solutions (pH 7.4) containing the various concentrations of glucose. As shown in Figure 6, at Nafion/GOx/MnO_2 NWs/GCE, the oxidation current around +0.65 V increased significantly with the increase of glucose concentration, while no obvious current response for glucose was observed at Nafion/GOx/GCE, indicating the successful fabrication of the glucose biosensor. In addition, we selected +0.65 V as the applied potential of chronoamperometry for the detection of glucose.

For the detection of glucose based the Nafion/GOx/MnO_2 NWs/GCE biosensor, chronoamperometry was performed at an applied potential of +0.65 V by the successive injection of

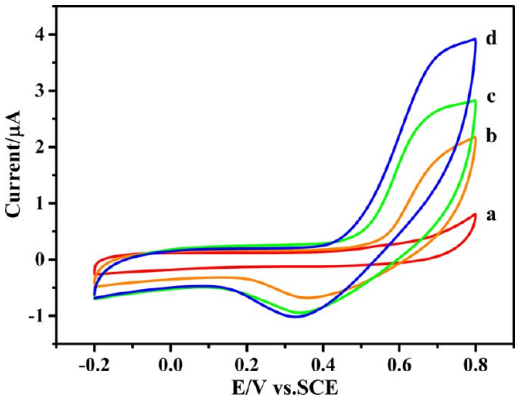

Figure 6. CV curves obtained at Nafion/GOx/GCE in PBS (pH 7.4) containing 0.2 mM glucose (a) and at Nafion/GOx/MnO_2 NWs/GCE sensor in PBS (pH 7.4) containing 0 (b), 0.1 (c), 0.2 mM glucose (d). Scan rate, 25 mV s^{-1}.

glucose (0−3 mM) into stirring PBS (pH 7.4). In the typical *i*−*t* curve (Figure 7A), 95% of steady-state current was reached in less than 5 s after successive injection of glucose, indicating the as-prepared biosensor exhibited a rapid response to glucose. The response time of 5 s in our case was shorter than those values of the GOx/MnO_2/field-effect transistor (140 s)[26] and GOx/Pt NPs/mesoporous carbon (15 s).[51] The calibration curve was plotted according to the current response (Figure

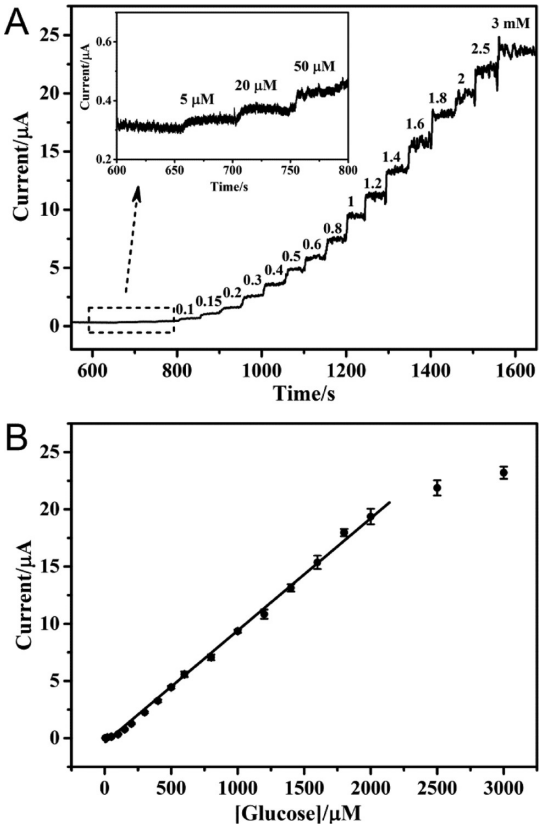

Figure 7. (A) Typical *i*−*t* curve obtained at Nafion/GOx/MnO_2 NWs/GCE sensor upon the successive injection of glucose in PBS solution, where the concentrations denote the final glucose concentration in the PBS after each injection of standard glucose solution. Applied potential: +0.65 V. (B) The calibration graph of the detection for glucose.

DOI: 10.1021/acsami.6b03266
ACS Appl. Mater. Interfaces XXXX, XXX, XXX−XXX

Table 1. Detection of Glucose in Real Samples Based on the Proposed Method

sample	known conc[c] (mM)	detected conc[d] (mM)	relative error	added (mM)	found[d] (mM)	recovery
1[a]	4.72	4.83 ± 0.21	+2.3%	2.00	6.91 ± 0.25	104%
2[a]	8.06	8.33 ± 0.28	+3.3%	2.00	10.26 ± 0.22	97%
3[b]	0.41	0.43 ± 0.02	+4.9%	2.00	2.47 ± 0.02	102%

[a]Human serum sample from local hospital. [b]Local peach juice. [c]The known concentrations of glucose were detected by commercial sensors. [d]All values were expressed as the mean ± standard deviation for three separate experiments.

7B). The linear regression equation is $y = 0.0099x - 0.5292$ ($R^2 = 0.9979$) with the linear range 5−2000 μM, which was wider than those values of GOx/MnO_2/field-effect transistor (25−1900 μM)[26] and GOx-Au-polydopamine/Fe_3O_4NPs/GCE (20−1875 μM).[52] The LOD was further estimated to be 1.8 μM glucose ($S/N = 3$), which was lower than that for reported enzymatic sensors based on ZnO/Cu nanocomposite (40 μM),[53] TiO_2 film (5.4 μM),[54] and Fe_3O_4 NPs (6.5 μM).[52] The proposed method was performed at the neutral pH, so as to avoid the alkaline condition where many transition metal oxides generally have electrochemical activities. Moreover, the detection was conducted in PBS containing 0.15 M NaCl, indicating that the sensor would work reliably for the real sample in the presence of chloride ions.

As the crucial parameters of a biosensor, the intra-assay and interassay reproducibility was investigated. On one hand, two different concentrations of glucose were detected for five replicate detections. The relative standard deviation (RSD) was 4.3% and 3.6% for 0.5 and 1 mM of glucose, respectively, indicating the good precision of the glucose biosensor. On the other hand, 1 mM of glucose was detected for three independent experiments by using different freshly prepared electrodes. The RSD was 3.9%, indicating acceptable reproducibility of the fabricated biosensor. In addition, no obvious decrease in the voltammetric response of sensor was observed after 3 days storage at 4 °C, and more than 90% of the original signal response was retained after 15 days, which was better or similar to that for reported biosensors, such as graphene/Nafion/GOD film-modified GCE (80% retained after 2 weeks)[55] and TiO_2/GOx/Nafion-modified GCE (94% retained after 2 weeks),[56] suggesting the long-term storage stability of the sensor.

To confirm the reliability and practicability, the fabricated sensor was used on the analysis of real samples. Prior to measurements, the samples were accurately diluted with PBS solution to fit into the linear range of calibration curve in Figure 7B. For each sample, three separate detections were conducted, and the concentrations of glucose were calculated on the basis of the work curve by multiplying the dilution ratios (Table 1). The results based on our method were in good agreement with the known results by general methods and the relative errors were within 4.9%. The recoveries were researched by the standard addition method and calculated to be 97−104%. These results demonstrated excellent precision, accuracy, and reliability of proposed method for the practical application.

4. CONCLUSIONS

In summary, the novel M13-templated MnO_2 NWs (20−30 nm in diameter and about 1 ± 0.1 μm in length) were synthesized through a facile biomineralization strategy. The synthesis mechanism was investigated, and the synthesis condition was optimized for obtaining the desired morphology. We found that as-prepared MnO_2 NWs exhibited high electrocatalytic activity at neutral pH. On the basis of the amperometric response for H_2O_2, a glucose biosensor was developed at neutral condition and showed a wide linear range (5 μM to 2 mM glucose), a low limit of detection of 1.8 μM glucose ($S/N = 3$), good reproducibility, and satisfactory storage stability. Due to the superiorities of synthesis and electrochemical performance, the phage-templated 1D NWs are promising to be applied in the bioanalysis, environmental monitoring, and energy storage.

AUTHOR INFORMATION

Corresponding Author

*E-mail: liuah@qdu.edu.cn.

Notes

The authors declare no competing financial interest.

ACKNOWLEDGMENTS

This work was financially supported in part by National Natural Science Foundation of China (Nos. 21275152, 21475144). We thank Dr. Hua He in China University of Petroleum for the zeta potential measurement and Prof. Mingdeng Wei in Fuzhou University, China, for XPS analysis.

REFERENCES

(1) Sui, N.; Duan, Y.; Jiao, X.; Chen, D. Large-Scale Preparation and Catalytic Properties of One-Dimensional α/β-MnO_2 Nanostructures. *J. Phys. Chem. C* **2009**, *113*, 8560−8565.

(2) Cheng, F.; Su, Y.; Liang, J.; Tao, Z.; Chen, J. MnO_2-Based Nanostructures as Catalysts for Electrochemical Oxygen Reduction in Alkaline Media. *Chem. Mater.* **2010**, *22*, 898−905.

(3) Pinaud, B. A.; Chen, Z.; Abram, D. N.; Jaramillo, T. F. Thin Films of Sodium Birnessite-Type MnO_2: Optical Properties, Electronic Band Structure, and Solar Photoelectrochemistry. *J. Phys. Chem. C* **2011**, *115*, 11830−11838.

(4) He, Y.; Chen, W.; Li, X.; Zhang, Z.; Fu, J.; Zhao, C.; Xie, E. Freestanding Three-Dimensional Graphene/MnO_2 Composite Networks As Ultralight and Flexible Supercapacitor Electrodes. *ACS Nano* **2013**, *7*, 174−182.

(5) Brock, S. L.; Duan, N.; Tian, Z. R.; Giraldo, O.; Zhou, H.; Suib, S. L. A Review of Porous Manganese Oxide Materials. *Chem. Mater.* **1998**, *10*, 2619−2628.

(6) Fennell, J. F.; Liu, S. F.; Azzarelli, J. M.; Weis, J. G.; Rochat, S.; Mirica, K. A.; Ravnsbæk, J. B.; Swager, T. M. Nanowire Chemical/Biological Sensors: Status and a Roadmap for the Future. *Angew. Chem., Int. Ed.* **2016**, *55*, 1266−1281.

(7) Li, L.; Nan, C.; Lu, J.; Peng, Q.; Li, Y. α-MnO_2 Nanotubes: High Surface Area and Enhanced Lithium Battery Properties. *Chem. Commun.* **2012**, *48*, 6945−6947.

(8) Cao, Y.; Xiao, L.; Wang, W.; Choi, D.; Nie, Z.; Yu, J.; Saraf, L. V.; Yang, Z.; Liu, J. Reversible Sodium Ion Insertion in Single Crystalline Manganese Oxide Nanowires with Long Cycle Life. *Adv. Mater.* **2011**, *23*, 3155−3160.

(9) Cheng, F.; Zhao, J.; Song, W.; Li, C.; Ma, H.; Chen, J.; Shen, P. Facile Controlled Synthesis of MnO_2 Nanostructures of Novel Shapes and Their Application in Batteries. *Inorg. Chem.* **2006**, *45*, 2038−2044.

(10) Liu, A. Towards Development of Chemosensors and Biosensors with Metal-Oxide-Based Nanowires or Nanotubes. *Biosens. Bioelectron.* **2008**, *24*, 167−177.

DOI: 10.1021/acsami.6b03266
ACS Appl. Mater. Interfaces XXXX, XXX, XXX−XXX

(11) Pan, Y.; Yi, W.; Hou, Z.; Liu, Y.-N. Green and Large-Scale One-Pot Synthesis of Small-Sized Graphene-Bridged Manganese Dioxide Nanowire Network as New Electrode Material for Electrochemical Sensing. *J. Sol-Gel Sci. Technol.* **2015**, *76*, 341−348.
(12) Kumar, N.; Dineshkumar, P.; Rameshbabu, R.; Sen, A. Morphological Analysis of Ultra Fine α-MnO_2 Nanowires under Different Reaction Conditions. *Mater. Lett.* **2015**, *158*, 309−312.
(13) Su, D.; Ahn, H.-J.; Wang, G. Hydrothermal Synthesis of α-MnO_2 and β-MnO_2 Nanorods as High Capacity Cathode Materials for Sodium Ion Batteries. *J. Mater. Chem. A* **2013**, *1*, 4845−4850.
(14) Grigorieva, A. V.; Melnik, D. M.; Goodilin, E. A.; Anufrieva, T. A.; Derlyukova, L. E.; Tretyakov, Y. D. Nanorods of Cryptomelane via Soft Chemistry Method and Their Catalytic Activity. *Solid State Sci.* **2012**, *14*, 988−995.
(15) Luo, J.; Zhu, H. T.; Fan, H. M.; Liang, J. K.; Shi, H. L.; Rao, G. H.; Li, J. B.; Du, Z. M.; Shen, Z. X. Synthesis of Single-Crystal Tetragonal α-MnO_2 Nanotubes. *J. Phys. Chem. C* **2008**, *112*, 12594−12598.
(16) Boppana, V. B. R.; Jiao, F. Nanostructured MnO_2: An Efficient and Robust Water Oxidation Catalyst. *Chem. Commun.* **2011**, *47*, 8973−8975.
(17) Dongale, T. D.; Jadhav, P. R.; Navathe, G. J.; Kim, J. H.; Karanjkar, M. M.; Patil, P. S. Development of Nano Fiber MnO_2 Thin Film Electrode and Cyclic Voltammetry Behavior Modeling Using Artificial Neural Network for Supercapacitor Application. *Mater. Sci. Semicond. Process.* **2015**, *36*, 43−48.
(18) Li, Z.; Ding, Y.; Xiong, Y.; Xie, Y. Rational Growth of Various α-MnO_2 Hierarchical Structures and β-MnO_2 Nanorods via a Homogeneous Catalytic Route. *Cryst. Growth Des.* **2005**, *5*, 1953−1958.
(19) Han, L.; Zhang, S.; Han, L.; Yang, D.-P.; Hou, C.; Liu, A. Porous Gold Cluster Film Prepared from Au@BSA Microspheres for Electrochemical Nonenzymatic Glucose Sensor. *Electrochim. Acta* **2014**, *138*, 109−114.
(20) Han, L.; Yang, D.-P.; Liu, A. Leaf-Templated Synthesis of 3D Hierarchical Porous Cobalt Oxide Nanostructure as Direct Electrochemical Biosensing Interface with Enhanced Electrocatalysis. *Biosens. Bioelectron.* **2015**, *63*, 145−152.
(21) Lang, X. Y.; Fu, H. Y.; Hou, C.; Han, G. F.; Yang, P.; Liu, Y. B.; Jiang, Q. Nanoporous Gold Supported Cobalt Oxide Microelectrodes as High-Performance Electrochemical Biosensors. *Nat. Commun.* **2013**, *4*, 2169.
(22) Dong, X. C.; Xu, H.; Wang, X. W.; Huang, Y. X.; Chan-Park, M. B.; Zhang, H.; Wang, L. H.; Huang, W.; Chen, P. 3D Graphene−Cobalt Oxide Electrode for High-Performance Supercapacitor and Enzymeless Glucose Detection. *ACS Nano* **2012**, *6*, 3206−3213.
(23) Pan, Y.; Hou, Z.; Yi, W.; Zhu, W.; Zeng, F.; Liu, Y.-N. Hierarchical Hybrid Film of MnO_2 Nanoparticles/Multi-Walled Fullerene Nanotubes−Graphene for Highly Selective Sensing of Hydrogen Peroxide. *Talanta* **2015**, *141*, 86−91.
(24) Li, L.; Du, Z.; Liu, S.; Hao, Q.; Wang, Y.; Li, Q.; Wang, T. A Novel Nonenzymatic Hydrogen Peroxide Sensor Based on MnO_2/Graphene Oxide Nanocomposite. *Talanta* **2010**, *82*, 1637−1641.
(25) Chen, J.; Zhang, W.-D.; Ye, J.-S. Nonenzymatic Electrochemical Glucose Sensor Based on MnO_2/MWNTs Nanocomposite. *Electrochem. Commun.* **2008**, *10*, 1268−1271.
(26) Luo, X.-L.; Xu, J.-J.; Zhao, W.; Chen, H.-Y. A Novel Glucose ENFET Based on the Special Reactivity of MnO_2 Nanoparticles. *Biosens. Bioelectron.* **2004**, *19*, 1295−1300.
(27) Sotiropoulou, S.; Sierra-Sastre, Y.; Mark, S. S.; Batt, C. A. Biotemplated Nanostructured Materials. *Chem. Mater.* **2008**, *20*, 821−834.
(28) Liu, Z.; Qiao, J.; Niu, Z.; Wang, Q. Natural Supramolecular Building Blocks: from Virus Coat Proteins to Viral Nanoparticles. *Chem. Soc. Rev.* **2012**, *41*, 6178−6194.
(29) Becerril, H. A.; Woolley, A. T. DNA-Templated Nanofabrication. *Chem. Soc. Rev.* **2009**, *38*, 329−337.
(30) Jolley, C. C.; Uchida, M.; Reichhardt, C.; Harrington, R.; Kang, S.; Klem, M. T.; Parise, J. B.; Douglas, T. Size and Crystallinity in Protein-Templated Inorganic Nanoparticles. *Chem. Mater.* **2010**, *22*, 4612−4618.
(31) Love, A. J.; Makarov, V.; Yaminsky, I.; Kalinina, N. O.; Taliansky, M. E. The Use of Tobacco Mosaic Virus and Cowpea Mosaic Virus for the Production of Novel Metal Nanomaterials. *Virology* **2014**, *449*, 133−139.
(32) Yang, D.-P.; Chen, S.; Huang, P.; Wang, X.; Jiang, W.; Pandoli, O.; Cui, D. Bacteria-Template Synthesized Silver Microspheres with Hollow and Porous Structures as Excellent SERS Substrate. *Green Chem.* **2010**, *12*, 2038−2042.
(33) Rosi, N. L.; Thaxton, C. S.; Mirkin, C. A. Control of Nanoparticle Assembly by Using DNA-Modified Diatom Templates. *Angew. Chem.* **2004**, *116*, 5616−5619.
(34) Jones, M. R.; Osberg, K. D.; Macfarlane, R. J.; Langille, M. R.; Mirkin, C. A. Templated Techniques for the Synthesis and Assembly of Plasmonic Nanostructures. *Chem. Rev.* **2011**, *111*, 3736−3827.
(35) Nam, K. T.; Peelle, B. R.; Lee, S.-W.; Belcher, A. M. Genetically Driven Assembly of Nanorings Based on the M13 Virus. *Nano Lett.* **2004**, *4*, 23−27.
(36) Nam, K. T.; Kim, D.-W.; Yoo, P. J.; Chiang, C.-Y.; Meethong, N.; Hammond, P. T.; Chiang, Y.-M.; Belcher, A. M. Virus-Enabled Synthesis and Assembly of Nanowires for Lithium Ion Battery Electrodes. *Science* **2006**, *312*, 885−888.
(37) Ghosh, D.; Lee, Y.; Thomas, S.; Kohli, A. G.; Yun, D. S.; Belcher, A. M.; Kelly, K. A. M13-Templated Magnetic Nanoparticles for Targeted in vivo Imaging of Prostate Cancer. *Nat. Nanotechnol.* **2012**, *7*, 677−682.
(38) Mao, C.; Liu, A.; Cao, B. Virus-Based Chemical and Biological Sensing. *Angew. Chem., Int. Ed.* **2009**, *48*, 6790−6810.
(39) Mao, C.; Solis, D. J.; Reiss, B. D.; Kottmann, S. T.; Sweeney, R. Y.; Hayhurst, A.; Georgiou, G.; Iverson, B.; Belcher, A. M. Virus-Based Toolkit for the Directed Synthesis of Magnetic and Semiconducting Nanowires. *Science* **2004**, *303*, 213−217.
(40) Lee, Y. J.; Yi, H.; Kim, W.-J.; Kang, K.; Yun, D. S.; Strano, M. S.; Ceder, G.; Belcher, A. M. Fabricating Genetically Engineered High-Power Lithium-Ion Batteries Using Multiple Virus Genes. *Science* **2009**, *324*, 1051−1055.
(41) Nam, K. T.; Lee, Y. J.; Krauland, E. M.; Kottmann, S. T.; Belcher, A. M. Peptide-Mediated Reduction of Silver Ions on Engineered Biological Scaffolds. *ACS Nano* **2008**, *2*, 1480−1486.
(42) Lee, Y.; Kim, J.; Yun, D. S.; Nam, Y. S.; Shao-Horn, Y.; Belcher, A. M. Virus-Templated Au and Au-Pt Core-Shell Nanowires and Their Electrocatalytic Activities for Fuel Cell Applications. *Energy Environ. Sci.* **2012**, *5*, 8328−8334.
(43) Liu, A.; Abbineni, G.; Mao, C. Nanocomposite Films Assembled from Genetically Engineered Filamentous Viruses and Gold Nanoparticles: Nanoarchitecture- and Humidity-Tunable Surface Plasmon Resonance Spectra. *Adv. Mater.* **2009**, *21*, 1001−1005.
(44) Velappan, N.; Fisher, H. E.; Pesavento, E.; Chasteen, L.; D'Angelo, S.; Kiss, C.; Longmire, M.; Pavlik, P.; Bradbury, A. R. M. A Comprehensive Analysis of Filamentous Phage Display Vectors for Cytoplasmic Proteins: an Analysis with Different Fluorescent Proteins. *Nucleic Acids Res.* **2010**, *38*, e22.
(45) Ramarajan, D.; Sivagurunathan, P.; Yan, Q. Synthesis and Characterization of Sol-Processed α-MnO_2 Nanostructures. *Mater. Sci. Semicond. Process.* **2012**, *15*, 559−563.
(46) Zhou, D.; Liu, Q.; Cheng, Q.; Zhao, Y.; Cui, Y.; Wang, T.; Han, B. Graphene-Manganese Oxide Hybrid Porous Material and Its Application in Carbon Dioxide Adsorption. *Chin. Sci. Bull.* **2012**, *57*, 3059−3064.
(47) Liu, D.; Zhang, Q.; Xiao, P.; Garcia, B. B.; Guo, Q.; Champion, R.; Cao, G. Hydrous Manganese Dioxide Nanowall Arrays Growth and Their Li^+ Ions Intercalation Electrochemical Properties. *Chem. Mater.* **2008**, *20*, 1376−1380.
(48) Dong, S.; Chen, X.; Gu, L.; Zhou, X.; Li, L.; Liu, Z.; Han, P.; Xu, H.; Yao, J.; Wang, H.; Zhang, X.; Shang, C.; Cui, G.; Chen, L. One Dimensional MnO_2/Titanium Nitride Nanotube Coaxial Arrays For High Performance Electrochemical Capacitive Energy Storage. *Energy Environ. Sci.* **2011**, *4*, 3502−3508.

DOI: 10.1021/acsami.6b03266
ACS Appl. Mater. Interfaces XXXX, XXX, XXX−XXX

(49) Xu, B.; Ye, M.-L.; Yu, Y.-X.; Zhang, W.-D. A highly sensitive hydrogen peroxide amperometric sensor based on MnO_2-modified vertically aligned multiwalled carbon nanotubes. *Anal. Chim. Acta* **2010**, *674*, 20−26.
(50) Wang, A.-J.; Zhang, P.-P.; Li, Y.-F.; Feng, J.-J.; Dong, W.-J.; Liu, X.-Y. Hydrogen peroxide sensor based on glassy carbon electrode modified with β-manganese dioxide nanorods. *Microchim. Acta* **2011**, *175*, 31−37.
(51) Yu, J.; Yu, D.; Zhao, T.; Zeng, B. Development of amperometric glucose biosensor through immobilizing enzyme in a Pt nanoparticles/mesoporous carbon matrix. *Talanta* **2008**, *74*, 1586−1591.
(52) Peng, H.-P.; Liang, R.-P.; Zhang, L.; Qiu, J.-D. Facile Preparation of Novel Core−Shell Enzyme−Au−Polydopamine−Fe_3O_4 Magnetic Bionanoparticles for Glucosesensor. *Biosens. Bioelectron.* **2013**, *42*, 293−299.
(53) Yang, C.; Xu, C.; Wang, X. ZnO/Cu Nanocomposite: a Platform for Direct Electrochemistry of Enzymes and Biosensing Applications. *Langmuir* **2012**, *28*, 4580−4585.
(54) Doong, R.-a.; Shih, H.-m. Array-Based Titanium Dioxide Biosensors for Ratiometric Determination of Glucose, Glutamate and Urea. *Biosens. Bioelectron.* **2010**, *25*, 1439−1446.
(55) Chen, X.; Ye, H.; Wang, W.; Qiu, B.; Lin, Z.; Chen, G. Electrochemiluminescence Biosensor for Glucose Based on Graphene/Nafion/GOD Film Modified Glassy Carbon Electrode. *Electroanalysis* **2010**, *22*, 2347−2352.
(56) Bao, S.-J.; Li, C. M.; Zang, J.-F.; Cui, X.-Q.; Qiao, Y.; Guo, J. New Nanostructured TiO_2 for Direct Electrochemistry and Glucose Sensor Applications. *Adv. Funct. Mater.* **2008**, *18*, 591−599.

DOI: 10.1021/acsami.6b03266
ACS Appl. Mater. Interfaces XXXX, XXX, XXX−XXX